Dielectric anisotropy, volume potential anomalies and the persistent Maxwellian equivalent body

2005 J. Phys.: Condens. Matter 17 7817

(http://iopscience.iop.org/0953-8984/17/50/004)

INSTITUTE OF PHYSICS PUBLISHING JOURNAL OF PHYSICS: CONDENSED MATTER

J. Phys.: Condens. Matter **17** (2005) 7817–7831 doi:10.1088/0953-8984/17/50/004

Dielectric anisotropy, volume potential anomalies and the persistent Maxwellian equivalent body

Margarita Simeonova and Jan Gimsa[1]

Chair of Biophysics, Department of Biology, University of Rostock, Gertrudenstraße 11A, D-18057, Rostock, Germany

E-mail: jan.gimsa@uni-rostock.de

Received 12 July 2005, in final form 20 September 2005
Published 2 December 2005
Online at stacks.iop.org/JPhysCM/17/7817

Abstract

Potentially, lipid membranes possess a high tangential conductivity and permittivity due to their surface charges and the in-plane orientation of the headgroup dipoles. Electrically, membranes exhibit a sandwich structure with a largely isotropic centre formed by the fatty acid chains and confined by two anisotropic headgroup layers. Accordingly, we described spherical vesicles by an aqueous core covered by three shells. For a theoretical comparison, models with an anisotropic single shell and anisotropic homogeneous spheres were also considered. Two effects can be clearly demonstrated. (1) High tangential conductivities or permittivities may lead to cyclic variations in the phase of the electric potential in the radial direction, resulting in a hemi-shell structure of the electric potential inside the objects with oppositely charged facets. The thickness of the anisotropic shell restricts the number of phase oscillations. (2) Despite the strong local field inhomogeneities, an isotropic homogeneous Maxwellian equivalent body with an identical external field distribution exists for any of the anisotropic models. Its properties can be found from a comparison of the numerically calculated surface potential and the classical expression of the Clausius–Mossotti factor at any given frequency. The permittivity conductivity pairs obtained exhibit a sigmoidal-like frequency dependence.

1. Introduction

Anisotropies denote orientation-dependent properties of matter. They are important for many physical and biological systems. While in biology electric anisotropies are well studied at the tissue level, comparatively little is known about anisotropies at the cellular and subcellular

[1] Author to whom any correspondence should be addressed.

levels. Nevertheless, electric anisotropies are observed in the cytoplasm, cytoskeleton, cell membranes, plant-cell walls, etc. The degree of anisotropy is determined by the physico-chemical structure and the arrangement of the constitutive molecules, e.g. microtubules, actin and myosin, structural polymers such as cellulose, membrane proteins or lipids.

The active electric properties of biological membranes are strongly anisotropic. Membrane-spanning protein channels transport ions in the normal direction, negligibly contributing to the tangential membrane conductance. The anisotropies in the passive electric properties of pure lipid membranes, i.e. conductivity and dielectric permittivity, are less apparent, and as a result often neglected. They arise from the structural peculiarities of the lipid molecules. The in-plane orientation of the polar lipid headgroups and their relatively free rotation contributes to the high tangential dielectric permittivity, which can exceed the normal component by a factor of ten [1–3]. Membrane surface charges lead to the adsorption and consecutive in-plane diffusion of ions, at several orders of magnitude higher than the rate of ion translocation through the non-polar membrane core. As a result, the tangential conductance is greatly increased [4].

These electric properties and the cell geometries determine their polarization by external electric fields. Cellular polarization gives rise to several AC-electrokinetic phenomena, like dielectrophoresis (DP), electro-rotation (ER), electro-deformation, etc [5–9]. For a theoretical description, dielectric cell models are employed. The common single-shell model (1SM) describes biological cells as spherical or ellipsoidal objects that consist of confocal layers like membrane and aqueous bulk media [10–12]. However, these models are highly simplified, since they neglect the structural complexity of the cellular media, assuming that the cytoplasm and membrane are isotropic and homogeneous.

As early as 1952, a field solution for homogeneous spheroidal objects (homogeneous model, HM) with anisotropic dielectric properties was found in crystal physics [13]. More recently, the solution has been extended to account for the electronic polarization of spherical [14] and ellipsoidal objects with an anisotropic coating [15, 16]. The same model has been used to describe the dielectric polarization of the 1SM [4]. The model successfully described the AC-electrokinetic behaviour of cells with anisotropic membrane properties, which were artificially induced by lipophilic ions [4, 17]. However, anisotropic dielectric cell models have so far considered mainly the surface polarization of the objects.

In this study, we have examined the mechanisms and patterns of the potential and polarization distributions within objects with anisotropic membrane properties. The original motivation of our study stemmed from the current discussions on the subcellular absorption of microwave field energy, as well as the expanding biotechnological applications of methods like electrofusion, trapping, and cell electroporation [18, 19]. We compared the solutions of the analytical Laplace equation with those of a numerical finite element method (FEM) for spherical object geometries. These considerations proved the correctness of Maxwell's notion of homogeneous equivalent bodies for anisotropic homogeneous models as well as for 1SMs with anisotropic media properties.

Naturally, the influence of the membrane dielectric properties on object polarization is enhanced for an increased ratio of membrane thickness to object radius. As a result, appropriate objects for the experimental verification of the effects of membrane anisotropy will probably be phospholipid vesicles with a size balanced between a high resolution of the dielectric membrane properties and the optical visibility of the object. We suggest dielectric single-object spectroscopy methods for the experimental verification of our theory, due to their higher resolution in object parameters. AC-electrokinetic methods can be expanded to small objects by light scattering [20] or by trapping fluorescence-labelled liposomes [21, 22].

2. Theory

2.1. Laplace equation

For biological objects with a magnetic permittivity close to unity and dimensions small compared to the electromagnetic wavelengths of interest, the electro-quasistatic (EQS) approximation can be applied [23]. For objects in aqueous solution with diameters of approximately 100 nm, this approximation will hold up to THz frequencies.

In EQS, the potential distribution Ψ induced by time harmonic fields is given by the Laplace equation:

$$\nabla \cdot [(\sigma + \mathrm{j}\omega\epsilon\epsilon_0)\nabla\Psi] = 0. \tag{1}$$

It depends on both the free and the displacement charges in the medium, expressed by its conductivity (σ) and dielectric permittivity (ϵ), respectively.

In general, σ and ϵ are second order dielectric tensors [14, 16, 23]. In most cellular membranes, σ and ϵ vary only in the normal (norm) and tangential (tang) directions with respect to the membrane surface [14, 16]. When the principal axes of the tensor coincide with the coordinate axes, the σ and ϵ tensors become diagonal. Diagonal tensors are obtained in spherical coordinates for spherically symmetric objects, where the norm and the tang components coincide with the radius vector and the angular coordinates, respectively. We will refer to this anisotropy as 'rotationally symmetric'.

2.2. Solution techniques

In the following, we present analytical and FEM solutions of the Laplace equation (equation (1)) for spherical objects with rotationally symmetric properties. The analytical solution was obtained in spherical coordinates. This is the classical solution for spherical objects, expressed in terms of spherical harmonics [24–26]. The potential within spherically symmetric anisotropic objects is radially modified by an effective number δ. For the 1SM with dielectrically anisotropic membrane, the solution is as follows [4, 14, 17]:

$$\begin{aligned}
\Psi_{\mathrm{ext}} &= (-E_0 r + A/r^2)\cos(\theta) \\
\Psi_{\mathrm{mem}} &= (-Br^{\delta} + C/r^{\delta+1})\cos(\theta) \\
\Psi_{\mathrm{int}} &= -Dr\cos(\theta).
\end{aligned} \tag{2}$$

The subscripts ext, mem and int stand for the exterior, membrane and interior, respectively. The anisotropy factor δ is complex and depends on the ratio of the normal and tangential components of the complex dielectric conductivity:

$$\delta = -\frac{1}{2} + \left[\frac{1}{4} + \frac{2\sigma^*_{\mathrm{tang}}}{\sigma^*_{\mathrm{norm}}}\right]^{1/2}. \tag{3}$$

The form of the coefficients A, B, C and D is found from the boundary conditions at the interface ($r = a$) of two media i and $i + 1$:

$$\begin{aligned}
&\Psi^*_i|_a = \Psi^*_{i+1}|_a \\
&\bar{\epsilon}^*_{n_i} \left.\frac{\partial E^*_i}{\partial r}\right|_a = \bar{\epsilon}^*_{n_{i+1}} \left.\frac{\partial E^*_{i+1}}{\partial r}\right|_a,
\end{aligned} \tag{4}$$

where r stands for the radius vector.

As an alternative approach we used the FEM method. It involves discretization of the Laplace equation into a problem with a finite number of unknown parameters. The starting point for FEM is a mesh that is a partition of the geometry into small units of simple shape.

The numerical solution is preferably applied for models of complex geometry and media properties. It provides a simultaneous solution for the frequency and the spatial dependences of the electrical quantities. In this work, we have used the FEM method for verification of the analytical solution as well as for a graphical representation of the potential distribution within the anisotropic models. The FEM solution was obtained in cylindrical coordinates, using the software FEMLAB©3.0.[2] The model objects were placed in the centre of a cylinder filled with external medium. To ensure a homogeneous external field, the radius and the height of the cylinder were five times larger than the vesicle radius. Its bases were equipotential planes, generating an electric field of 2.5×10^3 V m^{-1} along the cylinder axis. Using the axis-symmetry of the model geometry, the two-dimensional formulation of the Laplace equation (equation (1)) could be solved instead. Further, we assumed that the cylindrical axes coincide with the principal axes of the diagonal dielectric tensor (see section 2.1). Accordingly, the dielectric tensor for the numerical models along any axis was obtained by a multiplication of the diagonal tensor with the proper rotation tensor.

2.3. The Clausius–Mossotti factor (CMF)

Electric fields polarize biological cells. The effective cellular polarization (P_{eff}) is the volume integral of the local polarizations divided by the cell volume (V). It corresponds to the induced dipole charges at the surface of the object, i.e. the surface polarization, which generate the driving force in all AC-electrokinetic effects. The frequency dependence of P_{eff} is expressed by the Clausius–Mossotti factor (CMF*) as follows:

$$\vec{P}_{\text{eff}} = \epsilon_e \epsilon_0 \text{CMF}^* \vec{E}, \tag{5}$$

where $\epsilon_e\epsilon_0$ is the permittivity of the external medium and $\vec{E}$ is the external field vector. CMF* is directly related to the frequency dependence of the AC-electrokinetic effects [9, 18, 19]. For example, the real and imaginary parts of the CMF* are related to the frequency dependences of the DP and the ER spectra, respectively [7, 9, 27, 28]. The CMF* provides a convenient link between theoretical analyses and experimental measurements and can be used to compare different dielectric models.

The complex CMF* is determined by the dielectric medium properties, the geometry of the object and the frequency of the external field [5, 7, 18, 29, 27, 24]. For spherical objects it is given by

$$\text{CMF}^* = 3\frac{\epsilon^*_{\text{eff}} - \epsilon^*_e}{2\epsilon^*_e + \epsilon^*_{\text{eff}}}, \tag{6}$$

where ϵ^*_{eff} is the effective permittivity of the object. In confocally shelled objects, the effective permittivity ϵ^*_{eff} is a structure-dependent mixture of the permittivities of the shells and the interior of the object [18]. The concept of effective permittivity coincides with the notion of Maxwell for an equivalent body [30, 31]. The equivalent body is homogeneous and exists for all isotropic spherical objects with confocal geometries. For any given frequency, it has the same external geometry and polarization as the inhomogeneous object. Equivalent bodies will have isotropic properties and a homogeneous volume polarization, with an orientation parallel to the applied external field. This corresponds to a homogeneous local field that can be calculated from the quotient of the potential at the pole and the axis length.

Accordingly, an alternative expression for the CMF* is given in terms of potentials as follows [31]:

$$\text{CMF}^* = 3\left(\frac{\Psi^*_e - \Psi^*_c}{\Psi^*_e}\right), \tag{7}$$

[2] Femlab 3.0. FEMLAB GmbH, Berliner Strasse 4, D-37073 Göttingen, Germany. Email: info@femlab.de

Table 1. Model dielectric properties.

Dielectric properties		Single-shell model (1SM)			Homogeneous model (HM)	
		Membrane	Interior	Exterior	Interior	Exterior
Conductivity	σ_{norm}	7×10^{-7}	0.1	0.1	7×10^{-7}	0.1
	σ_{tang}	7; 0.7; 0.07			7; 0.7; 0.07	
Permittivity	ϵ_{norm}	3.7	78	78	3.7	78
	ϵ_{tang}	3700; 370; 37			3700; 370; 37	

where Ψ_c^* is the (complex) potential at a point on the surface of the object, e.g. its pole, and Ψ_e^* is the (real) potential at the same point in the absence of the object. The rotationally symmetric anisotropy does not influence the dependence of the potential on the angular component (θ) (see equation (2)). Therefore, equation (7) defines the same CMF* for any point at the outermost confocal surface of an object. (Since no potential is induced at points in the equatorial plane these are an exception. Please also note that the situation is more complex when the principal axes of the anisotropy are not in parallel to the field, e.g. for objects with Cartesian anisotropy.) This corresponds to a constant polarization, i.e. a constant local field, within a homogeneous, isotropic, equivalent body. To obtain the effective permittivity and conductivity of the equivalent body, the properties of the external medium as well as the real and the imaginary parts of the CMF* obtained by potential 'measurements' from equation (7) were employed in equation (6), respectively.

3. Models

Spherical models with rotationally symmetric properties are relevant to spherical biological cells, vesicles and some viruses. As a standard object geometry we assumed a sphere with an external radius of 75 nm. It was assumed to be suspended in an aqueous solution with a permittivity of 78 and a conductivity of 0.1 S m^{-1}.

A vesicle with a spherical core was assumed for the 1SM, surrounded by a 5.5 nm thick lipid membrane. For simplicity, the same dielectric properties were assumed for the core and the external medium. The isotropic membrane was characterized by a conductivity of 7×10^{-7} S m^{-1} and a permittivity of 3.7. In the anisotropic 1SMs, the membrane was anisotropic either in permittivity or conductivity. We considered various values for the tangential electric components. The reason is the membrane structure, giving rise to high tangential permittivities [1–3] and conductivities [4]. In the calculations, the normal components were left constant and equal to the isotropic parameters (table 1). For simplicity, all models were assumed to have frequency-independent permittivities and conductivities. In practice, it will be unrealistic to assume values as high as 3700 over a frequency band of nine decades. Dispersion processes will lead to a reduction of the high initial values and consequently roughly to a transition from the high to the low values given in table 1. Nevertheless, data on the dispersion frequencies are sparse [3].

To distinguish the dielectric from the geometric membrane effects, the 1SM was compared with a structurally homogeneous dielectric sphere (homogeneous model, HM) with internal properties equal to those of the anisotropic membrane (table 1).

The localization of the anisotropic properties in the lipid headgroup regions was taken into account by a three-shell model (3SM). Its membrane consisted of a central isotropic membrane

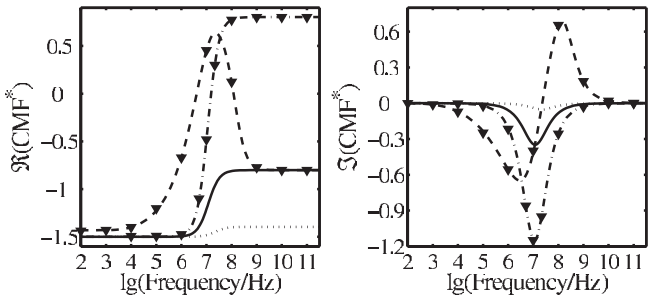

Figure 1. Comparison of the analytical solutions (lines) with the FEM solutions (triangles) for the anisotropic models. Real ($\Re$(CMF*)) and imaginary ($\Im$(CMF*)) parts of CMF* for an isotropic HM (· · · · · ·) and for 1SMs with homogeneous isotropic (——) and anisotropic membranes. In the anisotropic models, either the conductivity, $\sigma_{\text{norm}} = 7 \times 10^{-7}$ S m^{-1} and $\sigma_{\text{tang}} = 7$ S m^{-1} (- - - -), or the permittivity, $\epsilon_{\text{norm}} = 3.7$ and $\epsilon_{\text{tang}} = 3700$ (— · —), is anisotropic.

layer of 3.5 nm thickness and a permittivity and conductivity of 3.7 and 7×10^{-7} S m^{-1}, respectively. The central layer was confined by two 1 nm layers of equal but anisotropic dielectric properties.

4. Results

Figure 1 compares the CMF* spectra of isotropic and anisotropic models. The $\Re$(CMF*) of the isotropic HM exhibits two plateaus, determined by the ratios of the media conductivities and permittivities, respectively. A similar frequency behaviour is observed for the isotropic 1SM. Due to the equality of the external and internal media conductivities, the plateau, typically observed at intermediate frequencies for 1SM, vanishes. The higher effective permittivity of the 1SM determines a higher magnitude of the permittivity plateau. The real and the imaginary parts of the CMF* are related by the Kramers–Kronig relation [7]. Plateau transitions correspond to peaks in the $\Im$(CMF*) frequency spectrum. Their magnitudes are determined by the strength of the dispersions.

Obviously, anisotropic membrane properties dramatically change the CMF* spectra of the 1SM. This result has been confirmed by both the analytical and the numerical solutions (figure 1). A high tangential membrane conductivity leads to the appearance of an intermediate plateau and a corresponding peak in the $\Re$(CMF*) and $\Im$(CMF*) spectra, respectively. In contrast, assigning an anisotropic permittivity to the membrane leads only to quantitative changes of the spectra.

To get a better notion on the polarization mechanisms of anisotropic objects we varied the degree of anisotropy (table 1). Effects of a high tangential conductivity appeared at low and medium frequencies, whereas those of the high tangential permittivity were manifested in the highest frequency range (figure 2). Increasing the tangential conductivity of the membrane increases the magnitude and the width of the intermediate plateau in the real part of CMF*. An increased tangential permittivity leads to higher magnitudes of the permittivity plateaus. For both anisotropies, at high magnitudes of the tangential dielectric component, the CMF* of the anisotropic 1SM and the corresponding HM are very similar (figures 2(a) and (c)) if not identical (figures 2(b) and (d)).

The actual anisotropic structure of biological membranes has been considered by the 3SM, where the anisotropy is restricted to both membrane surfaces. We checked that under our conditions the outermost anisotropic shell dominates the electric behaviour of the object,

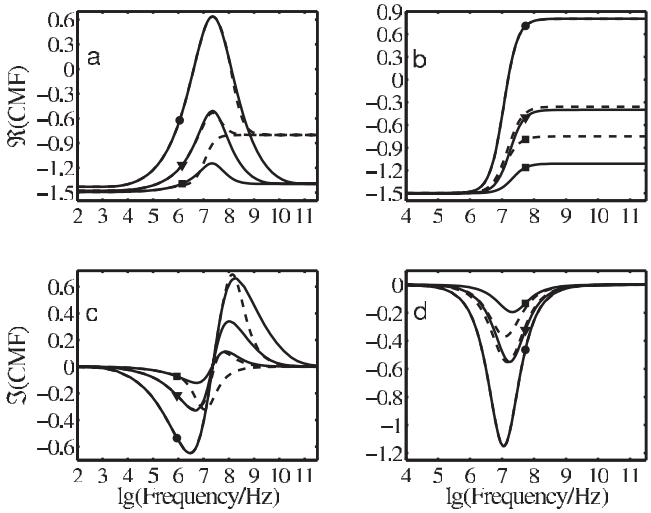

Figure 2. $\Re$(CMF*) and $\Im$(CMF*) for 1SMs (- - - -) and HM (——) with anisotropic membrane conductivities ((a), (c), $\sigma_{tang} = 7$ (circle), 7×10^{-1} (triangle) or 7×10^{-2} S m^{-1} (square)) and permittivities ((b), (d), $\epsilon_{tang} = 3700$ (circle), 370 (triangle) or 37 (square)).

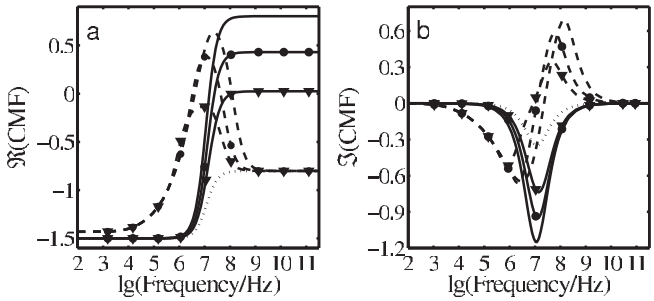

Figure 3. $\Re$(CMF*) and $\Im$(CMF*) of the isotropic 1SM (· · · · · ·) and anisotropic 1SM and 3SMs with either conductivity-, $\sigma_{tang} = 7$ S m^{-1} (- - - -), or permittivity-based, $\epsilon_{tang} = 3700$ (——), anisotropy. The anisotropic surface layers of the 3SMs are either 1 nm (circle) or 0.5 nm (triangle) thick.

i.e. the behaviour of the 3SM is equivalent to that of a 2SM, when assuming the properties of the central membrane layer also for the internal anisotropic layer. As expected, the reduction in the volume of the anisotropic membrane fraction results in a reduction of the anisotropy effects. This applies to models, no matter whether their anisotropy is conductivity or permittivity based, as expressed in the levels of the medium and high frequency plateaus of their $\Re$(CMF), respectively (figure 3(a)). For example, an anisotropic permittivity for a volume fraction of around 8% (0.5 nm anisotropic layer) in the outermost headgroup region results in an increase of the plateau level to more than 50% of the level for a completely anisotropic membrane.

The polarization patterns of the anisotropic models are determined by the potential distribution within the anisotropic media (figure 4). Surprisingly, the potential in the anisotropic HM does not decrease linearly towards the centre of the object but undergoes consecutive phase alterations of more than 180°. Accordingly, oppositely charged regions occur in a snapshot (figures 4(a) and (c)). Their width depends on the external frequency. The induced potentials have the highest magnitude along the radius line to the pole of the HM. They decline with

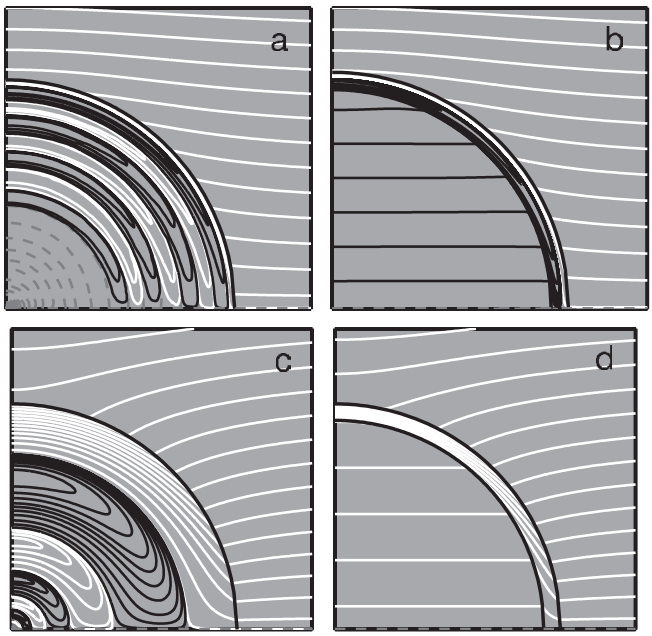

Figure 4. Distribution of the real part of the potential within the HM and the 1SM for $\sigma_{\text{norm}} = 7 \times 10^{-7}$ S m^{-1} and $\sigma_{\text{tang}} = 7$ S m^{-1} at 10 MHz ((a) and (b)) and 1 GHz ((c) and (d)), respectively. The external field is vertically oriented between the bottom (0 V) and the top (positive V) horizontal axes. The white lines are positive isopotential lines, the black are negative and the dashed lines are at 0 V. Please note that the distances between the isopotential lines are not to scale (compare to figure 5).

decreasing r and θ, i.e. towards the centre and the equatorial plane of the object, respectively. The oppositely charged areas are separated by zero-potential lines. An analogous potential distribution is observed in the anisotropic shells of the 1SM (figures 4(b) and (d)). This is also expected for the 3SM. However, the small thickness of the anisotropic layer restricts the number of cyclic phase oscillations. At 10 MHz, the membrane potential in the 1SM undergoes a single 180° phase shift and at the internal membrane surface it exhibits a negative amplitude. The continuity of the potential at the boundaries results in a core, oppositely charged with respect to the external potential. In contrast, at 1 GHz, the potential within the membrane does not exhibit any phase shift and the interior of the object is charged in phase with the external potential.

The frequency and the radial dependences of the induced potentials within the surface regions of the anisotropic 1SM and HM are depicted in figure 5. At low frequencies (1 kHz), the high tangential membrane conductivity causes the potential to decrease rapidly with decreasing distance, r. Therefore, even if the shift in the potential phase is considerable, the potential magnitude appears negligibly small (figure 5(a)). At higher frequencies the potential decreases over large distances. The first region, underneath the surface of the object with more than 180° potential shift, is clearly distinguishable and has a magnitude around ten times smaller than the potential at the surface. Note that the strong screening effect of the high tangential conductivity results in similar potential distributions within the HM and 1SM at 1 kHz and 1 MHz. Potential phase shifts can also be generated by high tangential permittivities. However, they appear at lower frequencies and have smaller magnitudes (figure 5(b)).

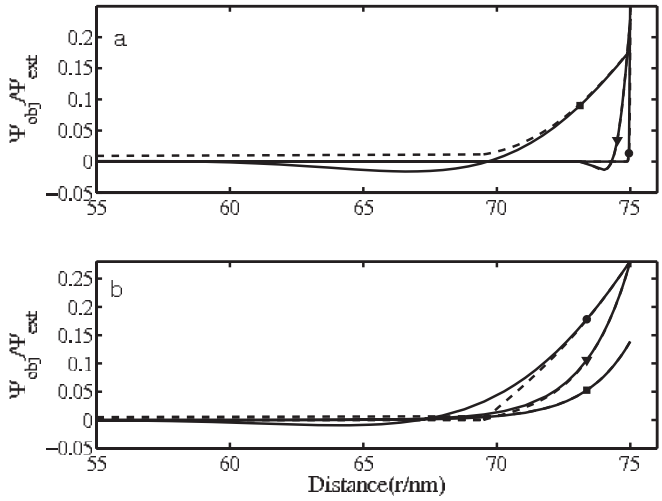

Figure 5. Real part of the potential along the polar radii of the 1SM (- - - -) and the HM (——) with anisotropic conductivity, $\sigma_{norm} = 7 \times 10^{-7}$ S m^{-1} and $\sigma_{tang} = 7$ S m^{-1} (a), and anisotropic permittivity, $\epsilon_{norm} = 3.7$ and $\epsilon_{tang} = 3700$ (b) at 1 kHz (circle), 1 MHz (triangle) and 1 GHz (square).

Despite the strong inhomogeneity of the potential distribution within their anisotropic media (figure 4), the HM, 1SM and 3SM exhibit a homogeneous surface polarization. Figure 6 shows the equivalent bodies of two anisotropic HMs. At 1 GHz, the polarization of the HM with a tangential conductivity of 7 S m^{-1} (figure 6(a)) is equivalent to the polarization of an isotropic HM with a conductivity and permittivity of 1.18 S m^{-1} and 20.086 (figure 6(b)), respectively. Analogously, at the same frequency a tangential permittivity of 3700 (figure 6(c)) in the same model geometry corresponds to an isotropic HM conductivity of 1.5×10^{-5} S m^{-1} and a permittivity of 163.63 (figure 6(d)). The equipotential planes within the equivalent bodies are always plane-parallel (homogeneous field).

The frequency dependences of the isotropic permittivities and conductivities of the equivalent bodies for all anisotropic model geometries have been found using the procedure described in section 2.3 (figure 7). Models with smaller degree of anisotropy have been used to allow for a better differentiation of the spectra (compare to figure 2). In all cases, the real parts of the equivalent conductivities and permittivities exhibit single sigmoidal-like transitions with increasing frequency. The equivalent permittivities and conductivities for the conductively anisotropic HM, 1SM and 3SM differ by less than one order of magnitude (figure 7(a)). However, the properties of the equivalent bodies for the models with anisotropic permittivities, exhibited significant magnitude differences as well as different frequency dependences (figure 7(b)).

5. Discussion

5.1. Oscillating potentials

5.1.1. Potential in anisotropic HM. The appearance of cyclic oscillations of the potential phase within anisotropic media (figure 4) results from the Laplace equation. The potential in the anisotropic HM is

$$\Psi_{int} = Ar^{\delta}\cos(\theta), \tag{8}$$

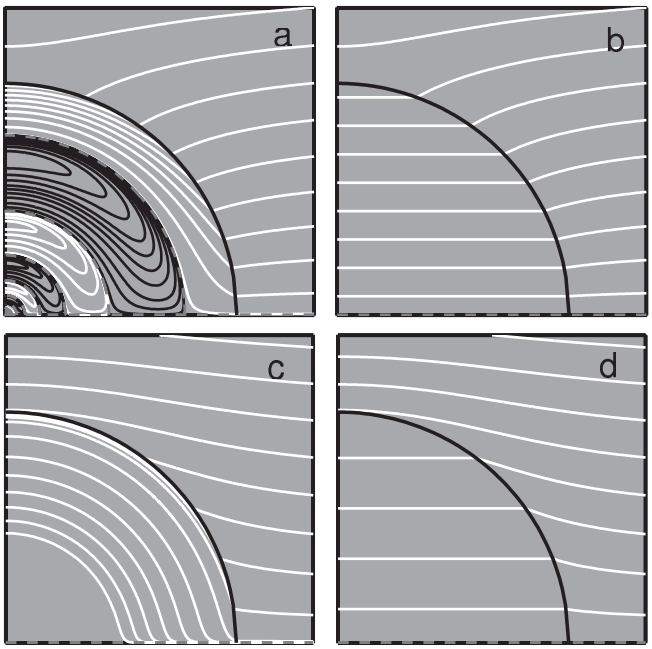

Figure 6. Distribution of the real part of the potential at 1 GHz within HMs with anisotropic conductivity ((a), $\sigma_{norm} = 7 \times 10^{-7}$ S m^{-1}, $\sigma_{tang} = 7$ S m^{-1}) or permittivity ((c), $\epsilon_{norm} = 3.7$ and $\epsilon_{tang} = 3700$) and their equivalent bodies ((b) and (d)). For details see figure 4. Please note the identity of the external potential distribution of the anisotropic objects and their equivalent bodies.

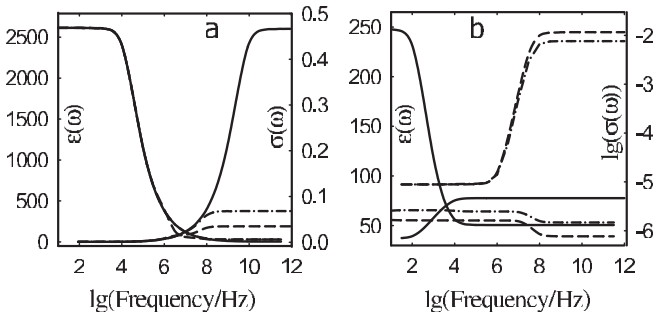

Figure 7. Frequency dependence of the equivalent conductivities (right scale) and permittivities (left scale) of the HM (——), 1SM (— · —) and 3SM (- - - -) with either anisotropic conductivity, $\sigma_{tang} = 7 \times 10^{-1}$ S m^{-1} (a), or anisotropic permittivity (b), $\epsilon_{tang} = 370$.

where δ was defined in equation (3). For $r > 0$, equation (8) can be transformed into

$$\Psi_{int} = ar^{\Re(\delta)} \cos(\theta)\{\sin[\alpha + |\Im(\delta)| \ln(r)] + j \cos[\alpha + |\Im(\delta)| \ln(r)]\}, \tag{9}$$

where $(ar^{\Re(\delta)} \cos(\theta))$ and $(\alpha + |\Im(\delta)| \ln(r))$ are the amplitude and the phase of the potential; a and α are frequency-dependent variables, whose values are related to $\Re(\delta)$ and $\Im(\delta)$, respectively. For a decreasing distance r, i.e. moving from the surface to the centre of the object, the amplitude of the potential decreases with $r^{\Re(\delta)}$ whereas the spatial density of phase oscillations increases. The spatial variations are further modified by the dielectric properties of the anisotropic media, represented by the anisotropy factor δ.

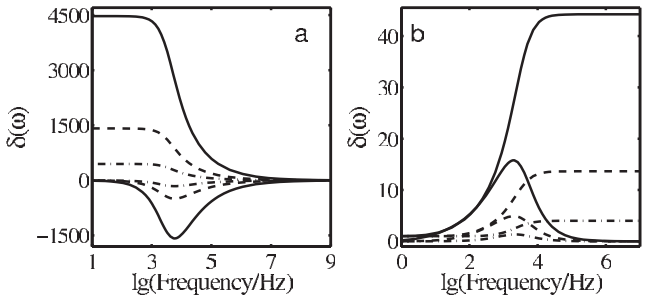

Figure 8. Frequency dependence of the real (sigmoidal) and the imaginary (peak) parts of the dielectric factor $\delta(\omega)$ for varying tangential conductivities (a), $\sigma_{\text{tang}} = 7$ (——), 7×10^{-1} (- - - -) and 7×10^{-2} (— · —) S m^{-1}, and permittivities (b), $\epsilon_{\text{tang}} = 3700$ (——), 370 (- - - -) and 37 (— · —).

Interestingly, the frequency-dependent function $\Re(\delta)$ undergoes a single sigmoidal transition that corresponds to a peak in the $\Im(\delta)$-function (figure 8). Each $\Re-\Im$ pair of these functions is very similar in shape to Lorentzian spectra. The frequency dependence of $\delta(\omega)$ appears independent of the tangential parameters. Nevertheless, its magnitude is higher for higher tangential conductivities or permittivities (figure 8). By contrast, an increase in the normal conductivity and permittivity increases and decreases the characteristic frequency of $\delta(\omega)$ dispersion, respectively. The dispersion magnitude remains unaffected (curves not shown). In summary, it is important how the degree of anisotropy is changed. However, biological membranes will exhibit more pronounced alterations in the permittivity and conductivity in the tangential than in the normal direction.

The decrease in the magnitude of the potential inside the object moving towards its centre is steeper for high $\Re(\delta)$ values (equation (8)). The maximum attenuation of potential in the surface region of the HM occurs at opposite ends of the frequency window, in accordance with the inverse frequency dependences of the $\Re(\delta)$ for the conductivity and permittivity based anisotropies (figure 8). Accordingly, the potential oscillations in the volume of the HMs with high tangential conductivity are less screened at higher frequencies, whereas they can be better revealed at low frequencies in the model with high tangential permittivity (figure 5). In both cases however, the density of the potential oscillations, given by the absolute magnitude of $\Im(\delta)$, is already decreased. For the anisotropic conductivities and permittivities used in our dielectric models (table 1), the maximum densities, i.e. the peaks of $\Im(\delta)$, occurred at around 6 and 2 kHz, respectively. We compared these frequencies to the limiting Maxwell–Wagner frequencies that can be obtained from each of the permittivity–conductivity pairs in the anisotropic model. In any case, the $\Im(\delta)$ maxima were below the lowest Maxwell–Wagner frequency.

5.1.2. Potential in the anisotropic 1SM. The potential distribution in the anisotropic shell of the 1SM arises from the contributions of the external field and the dipole field of the polarized core. In the radial direction, both terms are modified by the same factor δ (see equation (3)). Under the condition of positive r, the potential in the anisotropic shell can be represented in analogy to equation (9) as

$$\Psi_{\text{shell}} = ar^{\Re(\delta)}\cos(\theta)\{\sin[\alpha + |\Im(\delta)|\ln(r)] + \mathrm{j}\cos[\alpha + |\Im(\delta)|\ln(r)] + \cdots + br^{1-\Re(\delta)}\cos(\theta)\{\sin[\beta + |\Im(\delta)|\ln(r)] + \mathrm{j}\cos[\beta + |\Im(\delta)|\ln(r)]\}. \quad (10)$$

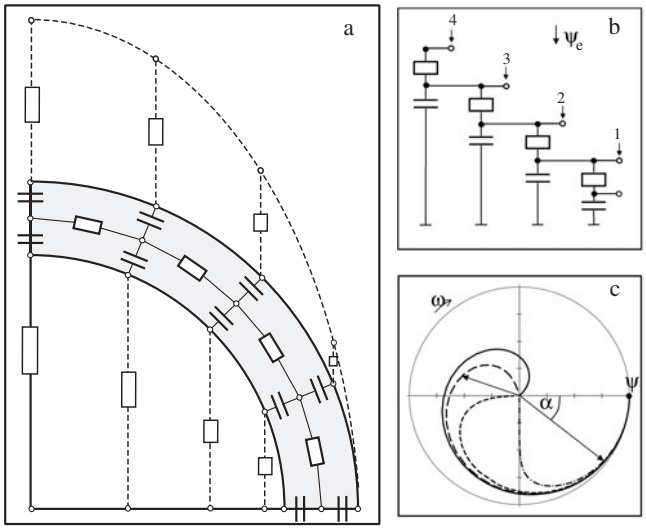

Figure 9. (a) 1SM with membrane of enhanced tangential conductivity (shaded area). The pole of the cell is towards the top of the figure. The external side of the membrane is charged by the external potential via the resistivity of the external medium, whereas the inner side is grounded (0 V) to the equatorial plane by the core resistivity. (b) RC phase shifter, producing a phase shift of more than 270°. The phase-shift (angle, α) of the potential, created by one (— · —), two (- - - -), three (– – –) or four (——) RC pairs, is presented in a polar plot (c).

For corresponding anisotropies, the variables a and α in the external-field term take the same values in the HM and in the shell of the 1SM. However, the dipole field term increases as one gets closer to the vesicle core, as well as for certain frequencies in the models with high tangential conductivity or permittivity. This leads to a deviation of the potential distribution within the anisotropic 1SM from the corresponding HM (figure 5).

The potential in the anisotropic layers of the 3SM can also be expressed by equation (10). Since the anisotropic layers are significantly thinner than the membrane in the 1SM, the influence of the core polarization is very strong. Potential phase oscillations with a radial period larger than the thickness of the anisotropic layers cannot be observed.

5.1.3. Mechanisms. The occurrence of spatially alternating potentials within the anisotropic media can be explained qualitatively by the RC (resistor–capacitor) scheme in figure 9(a). The scheme considers the effects of an enhanced tangential conductivity.

For example, the peak of the negative phase of the external AC potential (or field) should be considered. The charge will be highest at the pole. (Please note that the actual peak value at the membrane surface may shift slightly in phase.) The centre plates of the top membrane-spanning capacitor pairs will be negatively charged. From here, negative charges are conducted to the centre plates of the other membrane-spanning capacitor pairs through the cascade of the tangentially oriented resistors. In this model, charges are also injected through the other external resistors, nonetheless with reduced contributions towards the model's equator. Finally, the centre plates of the capacitors form negative depots of charges, with charge numbers decreasing from the pole along the arc of the membrane (figure 4). For symmetry reasons, the voltage must be zero at the equatorial plane. With the rising positive flank of the external AC potential, positive charges are deposited in the membrane, first neutralizing the negatively charged depots. The RC relaxation time inside the membrane introduces a phase shift of the

inner membrane potential. The magnitude of the out-of-phase component of the potential is at a maximum when the external field frequency and the RC relaxation time match. As in the 1SM, oppositely charged areas cannot be observed at DC and at very high frequencies (figure 8(a)).

Qualitatively, the RC scheme in figure 9(a) functions analogously to the RC phase shifter in figure 9(b) that is widely used in electronic circuitry. In principle, a single RC pair may induce a maximum phase shift of 90° (though at zero amplitude). Accordingly, two cascaded RC pairs may induce up to 180° and so on. This means that a minimum of three RC pairs are required to create a charge depot with a phase shift of more than 180°, i.e. having a sign opposite to that of the externally applied potential. Figure 4 shows an 'effective number of RC pairs' higher than three for anisotropic membrane models.

One has to consider a multitude of RC phase shifters to model the occurrence of more than one cyclic phase oscillation within the anisotropic medium. For example, 'concentric layers' of RC phase shifters must be assumed in the volume of anisotropic HMs. Most of the charges will be deposited below the model's surface, leading to the highest potential amplitude in the first 'layer'.

Analogously, the occurrence of a potential phase shift can be explained in models with enhanced tangential permittivity. However, whereas the above RC phase shifters represent low-pass filters, the exchange of the resistors for capacitors and vice versa inside the membrane leads to a high-pass characteristic in these models (compare to figure 8). We found a lower number of cyclic phase oscillations for our models with anisotropic permittivity (figure 8(b)).

5.2. Equivalent body

The notion of equivalent bodies was originally developed by Maxwell [30] for spherically symmetric, homogeneous or confocally shelled objects with isotropic dielectric properties. In dielectric media with radially symmetric anisotropy only the radial and not the angular components of the local field are modified. As a result, the volume polarization of anisotropic objects appears inhomogeneous (figure 4) even though their surface exhibits a polarization pattern corresponding to homogeneous isotropic objects (figure 6). For this reason, Maxwell's notion can be extended to objects made of anisotropic media. This also applies to anisotropic 1SMs and 3SMs, which can be described by equivalent isotropic HMs. The similarity of the CMF* spectra of the anisotropic HM, 1SM and 3SM at high magnitudes of the tangential dielectric components (figures 2 and 3) suggests similar properties of their equivalent bodies. For small anisotropies, the polarization of the models is very similar to that of isotropic objects (figure 1).

We have further tried to extend Maxwell's notion to an isotropic 'equivalent membrane'. Assuming the same core properties and following the procedure in section 2.3, we tried to find the permittivity and conductivity for the isotropic shell of the 'equivalent 1SM' for every frequency. However, such an 'equivalent membrane' could not be found for every frequency. Most probably this is due to the influence of the anisotropic shell on the polarization of the core. A phase shift of the local field of more than 90° with respect to the external field can only be observed in 1SMs with anisotropic membrane (figure 4(b)). Therefore, the assumption of the same core properties for a model with an anisotropic shell and an 'equivalent 1SM' with an isotropic shell seems to be inconsistent.

6. Conclusions

We could show that the surface polarization of radially symmetric anisotropic objects is equivalent to the polarization of homogeneous isotropic objects, i.e. Maxwellian equivalent

bodies exist. The frequency dependence of the conductivity and permittivity of the equivalent bodies exhibit 'relaxations' with a single time constant. This equivalence may result in erroneous interpretations of impedance or AC-electrokinetic data of biological objects.

Since dielectric particle or cell characterization and manipulation methods are based on surface polarization (which is equivalent to the induced dipole moment, compare equations (6) and (7)), the anomalous potential distribution within the volume of the objects remains completely hidden. This may explain why anisotropy effects have rarely been detected. Nevertheless, the frequency dependence of the object properties that are introduced by possible anisotropies will influence the electro-manipulation and handling properties of particles in biotechnological applications.

Even though dispersion processes in anisotropic (biological or colloidal) objects are based on the structure of the objects, they possess properties that are qualitatively different from common structural dispersions. Firstly, in practice, the anisotropic properties are introduced by the molecular structure of the objects and therefore strongly related to molecular properties, and secondly, they generate an electrical 'fine structure' inside homogeneous media as can be seen in HMs.

Furthermore, dielectric anisotropies may lead to a strong inhomogeneity of the potential and field distributions in homogeneous media, especially in the surface regions of spherical HMs and 1SMs. High local fields in these regions may induce large currents leading to a localized field absorption and consequent energy dissipation.

Acknowledgments

MS is grateful for a grant from the Deutscher Akademischer Austauschdienst (German Academic Exchange Service). This study has been supported by grant StSch 2002 0418A from the Bundesamt für Strahlenschutz (Federal Office for Radiation Protection). We are grateful to J Flehr, Dr U Schreiber and D Wachner for technical assistance. Dr U Gimsa and R Sleigh are acknowledged for help with the manuscript.

References

[1] Raudino A and Mauzerall D 1986 *Biophys. J.* **50** 441–50
[2] Stern HA and Feller S 2003 *J. Chem. Phys.* **118** 3401–12
[3] Klösgen B, Reichle C, Kohlsmann S and Kramer K 1996 *Biophys. J.* **71** 3251–60
[4] Sukhorukov V, Meedt G, Kürschner M and Zimmermann U 2001 *J. Electrostat.* **50** 191–204
[5] Pohl H 1978 Dielectrophoresis *The Behavior of Neutral Matter in Nonuniform Electric Fields* (Cambridge: Cambridge University Press)
[6] Zimmermann U and Arnold W 1983 *Coherent Excitations in Biological Systems* ed H Fröhlich and F Kremer (Berlin: Springer) pp 211–21
[7] Pastushenko V, Kuzmin P and Chizmadshev Yu 1985 *Stud. Biophys.* **110** 51–7
[8] Delgado A 2001 *Interfacial Electrokinetics and Electrophoresis* (New York: Dekker)
[9] Gimsa J 2001 *Bioelectrochemistry* **54** 23–31
[10] Hagedorn R and Fuhr G 1984 *Stud. Biophys.* **102** 229–39
[11] Fuhr G, Gimsa J and Glaser R 1985 *Stud. Biophys.* **108** 149–64
[12] Sauer F and Schlögl R 1985 *Interactions Between Electromagnetic Fields and Cells* ed A Chiabrera, C Nicolini and H Schwan (New York: Plenum) pp 203–51
[13] Cade R 1952 *Proc. Phys. Soc.* **LXVI** 557–69
[14] Lucas A, Henrard L and Lambin P 1994 *Phys. Rev.* B **49** 2888–96
[15] Ambjörnsson T and Mukhopadhyay G 2003 *J. Phys. A: Math. Gen.* **36** 10651–65
[16] Ambjörnsson T and Apell S P 2004 *Phys. Rev.* E **69** 031914:1–7
[17] Ko Y, Huang J and Yu K 2004 *J. Phys.: Condens. Matter* **16** 499–509
[18] Jones T 1995 *Electromechanics of Particles* (Cambridge: Cambridge University Press)

[19] Zimmermann U and Neil G 1996 *Electromanipulation of Cells* (Boca Raton, FL: CRC Press)
[20] Gimsa J 2001 *Interfacial Electrokinetics and Electrophoresis* ed A Delgado (New York: Dekker) pp 369–400
[21] Müller T, Gerardino A, Schnelle T, Shirley S, Bordoni F, Degasperis G, Leoni R and Fuhr G 1996 *J. Phys. D: Appl. Phys.* **29** 340–9
[22] Green N and Morgan H 1997 *J. Electrostat.* **42** 279–93
[23] Van Rienen U, Flehr J, Schreiber U and Motrescu V 2003 *International Series of Numerical Mathematics* vol 146 (Basel: Birkhäuser) pp 17–31
[24] Stratton J 1941 *Electromagnetic Theory* (New York: McGraw-Hill)
[25] Laud B 1987 *Electromagnetics, A Halsted Press Book* 2nd edn (New York: Wiley)
[26] Landau L and Lifschitz E 1985 *Elektrodynamik der Kontinua* vol 8 (Berlin: Akademie)
[27] Gimsa J, Marszalek P, Loewe U and Tsong T 1991 Dielectrophoresis and electrorotation of neurospora slime and murine myeloma cells *Biophys. J.* **60** 749–60
[28] Wang X, Huang Y, Hölzel R, Burt J and Pethig R 1992 *J. Phys. D: Appl. Phys.* **26** 312–22
[29] Grosse C 2001 *Interfacial Electrokinetics and Electrophoresis* ed A Delgado (New York: Dekker) pp 277–326
[30] Maxwell J 1873 *Treatise on Electricity and Magnetism* (London: Oxford University Press)
[31] Gimsa J and Wachner D 1999 *Biophys. J.* **77** 1316–26